
Article:
Huang, S-S., Burgess, I., Huang, Z. et al. (1 more author) (2011) The mechanics of inelastic buckling using a Shanley-like model. Proceedings of the Institution of Civil Engineers: Engineering and Computational Mechanics, 164 (2). 103 - 119. ISSN 1755-0777

https://doi.org/10.1680/eacm.2011.164.2.103

---

11 March 2010

The mechanics of inelastic buckling using a Shanley-like model

Dr. Shan-Shan Huang
BEng, MSc, PhD
Research Assistant
Department of Civil and Structural Engineering, The University of Sheffield, Sir Frederick Mappin Building, Mappin Street, Sheffield, S1 3JD, UK
Tel: +44 114 2225726
E-mail: s.huang@shef.ac.uk

Prof. Ian Burgess
BA, PhD, CEng, MIStructE
Professor of Structural Engineering
Department of Civil and Structural Engineering, The University of Sheffield

Dr. Zhaohui Huang
BEng, PhD
Lecturer
Department of Civil and Structural Engineering, The University of Sheffield

Prof. Roger Plank
BSc, PhD, CEng, MICE, FIStructE
Professor
School of Architecture, The University of Sheffield

Number of words: 5344
Number of figures: 17
Number of tables: 2

Abstract

This paper presents a study of the mechanics of inelastic buckling using a Shanley-like simplified column model. The model is an extension of the original Shanley model with multiple springs and two dampers. The inclusion of damping enables the dynamic response of the model under constant loading to be captured. The model has been evaluated against the tangent-modulus and reduced-modulus critical buckling loads, and has been found effective in representing the progressive change in the regions of loading and unloading during inelastic buckling. It is also able to simulate the extreme situations of inelastic buckling by varying the ratio of the two damping coefficients. It is seen that high rotational damping, relative to vertical damping, causes the buckling to move towards the reduced-modulus buckling load at much lower deflections than when the relationship is reversed.

Notation

F critical buckling load

I second moment of area of the column cross section

l column length

E Young's modulus

E_t tangent modulus

E_r reduced modulus

P applied load

F_{sij} reaction force on spring j ($j = 1, n$ from column centre to edge) on either left-hand side ($i = 1$) or right-hand side ($i = 2$)

F_{cv} reaction force on the vertical damper

θ_0 initial imperfection

L model length

B model width

M_{cr} reaction moment on the rotational damper

C_v damping coefficient of the vertical damper (Ns/mm)

C_r damping coefficient of the rotational damper (Nmms)

u vertical moment

θ rotation

$\dot{u}$ velocity of u

$\dot{\theta}$ velocity of θ

k stiffness at linear-elastic stage

k_t stiffness at plastic stage, set to be 25% of k

F_p spring force at proportional limit

x_p spring deformation at proportional limit ($x_p = F_p / k$)

F_{UL} spring force when unloading starts

x_{UL} spring deformation when unloading starts

P_t tangent-modulus load

P_r reduced-modulus load

$\tilde{\theta}$ an arbitrary small rotation

ΔF_{sij} additional F_{sij} caused by the rotation $\tilde{\theta}$

Δx_{ij} additional deformation of spring j ($j = 1, n$ from column centre to edge) on either left-hand side ($i = 1$) or right-hand side ($i = 2$) caused by the rotation $\tilde{\theta}$

R_d relative damping ratio

Key words: Columns, Fire Engineering, Mathematical Modelling

1 Introduction

Simplified models are often very efficient in clarifying structural behaviour, in particular when the underlying mechanics is of interest. For column buckling in the inelastic range, the model due to Shanley (1947) is perhaps the best known, and probably the most effective, discrete model. Shanley reconciled the controversy between the tangent-modulus (Engesser 1889) and the reduced-modulus (Considère 1891) theories, and pointed out the non-uniqueness of the critical buckling loads in inelastic buckling. This phenomenon is well demonstrated by Shanley's simple column model, which has been used, occasionally in modified form, by other authors in studies related to inelastic buckling (for example Genna & Symonds 1987, Massin *et al.* 1999, Corona 2001 and Little 2004).

The use of very slender concrete and composite columns is rapidly growing in buildings, especially in non-seismic regions such as the UK. Concrete, the main material of such columns, has a relatively newly-found property at high temperatures, defined either as Transient Strain (TS) or as Load-Induced Thermal Strain (LITS). (Anderberg & Thelanderson 1976, Khoury *et al.* (1985a, b, 1996, 2006) Schneider & Horvath 2003) Although a slender concrete or composite column subject to an accidental fire is surely vulnerable to TS, the way in which the phenomenon affects buckling in such cases is not known and in need of investigation. In order to investigate the problem in terms of its underlying mechanics, as a preliminary to a more detailed analysis of concrete columns in fire, a simplified column model has therefore been used. In this paper, the modified Shanley model is presented. The original two-

spring discrete model is extended by adding more springs, in order to create a more continuous stress distribution through the cross-section. Since the relative-rate dependency of the inelastic buckling behaviour is of interest, the model has been set up with two dampers, one for each degree of freedom. The effect of the relative rates of the two DoFs has been examined by varying the ratio of the damping coefficients.

2 Historical review of inelastic buckling theories

If imperfection effects are set aside, the strength of a column depends on its geometry (slenderness ratio) and its material properties (stiffness and strength). Very slender columns fail by buckling when the material is still linear-elastic (elastic buckling), and the classic Euler formula is applicable in the determination of the critical buckling load. In contrast, very stocky columns fail by yielding and crushing of the material, and hence their strength depends solely on the ultimate compressive strength of the material; no consideration of buckling or stability is necessary. Between these extremes, for columns with intermediate slenderness, buckling occurs after the material has become plastic but before it crushes, which is known as inelastic buckling (Gere & Timoshenko 1997). In this case, the simple elastic buckling solution is no longer valid, and the inelastic behaviour of the material must be taken into account. The slenderness of composite columns very often lies in the 'intermediate' range, and so their global failure mode will commonly be inelastic buckling.

Various inelastic buckling theories have been published since the late 1880s, including the tangent-modulus theory, the reduced-modulus theory and

Shanley's theory (Shanley 1947, Bleich 1952, Bazant & Cedolin 1991). Both the tangent-modulus and reduced-modulus theories assume that inelastic buckling has characteristics analogous to elastic buckling. It is assumed that the column fails by buckling at a constant load from a neutrally stable equilibrium state. This critical load is determined by generalizing Euler's formula with changed elastic modulus.

In the tangent-modulus theory, Young's modulus E is replaced by a tangent modulus E_t, which is the gradient of the compressive stress-strain curve at the critical stress (Gere & Timoshenko 1997). This theory oversimplifies inelastic buckling by using a unique tangent modulus. In reality, the tangent modulus depends on the concurrent strain levels, which vary through the cross-section and may even be subject to elastic strain reversal on the convex side of the member due to bending.

The reduced-modulus theory attempts to mitigate the error of neglecting strain-rate reversal on the convex side of a deflected column in the tangent-modulus theory. It considers both increasing strain with tangent modulus E_t on the concave side, and decreasing strain with Young's modulus E on the convex side when buckling occurs. An effective modulus (known as the reduced modulus E_r), which lies between E and E_t, is introduced to replace E_t in the tangent-modulus formula (Bazant & Cedolin 1991).

The three basic column formulas may be written as follows (assuming pinned ends and zero eccentricity):

Euler	$F_e = \pi^2 EI/l^2$	(1)
Tangent modulus	$F_t = \pi^2 E_t I/l^2$	(2)
Reduced modulus	$F_r = \pi^2 E_r I/l^2$	(3)

However, whether a perfect column will remain straight until its deflection suddenly bifurcates at a certain critical load (shown as the straight horizontal lines in Fig. 1) in the inelastic range is questionable. Shanley (1947) showed from tests and a simplified mathematical analysis that, unlike elastic buckling, inelastic buckling does not have a unique critical load. The column starts to buckle at the tangent-modulus critical load, and the buckling proceeds simultaneously with further increase of axial load, but the load does not exceed the reduced-modulus load, shown as the rising curve in Fig. 1.

It is also logical to state that the manner of inelastic buckling significantly depends on the relative rates of change of the axial and bending strains. When a column starts to deflect laterally the strains through a cross-section due to axial compression and to bending are superposed. If the axial strain at all points through the cross-section is imposed more rapidly than the bending strain then it is possible for buckling to occur without strain reversal, as described in the tangent-modulus theory. On the other hand, if the column deflects so rapidly that only the high stiffness given by reversal can keep the load constant, then what is described as the reduced-modulus theory would apply. These two theories give the two practical extremes of inelastic buckling. Between these two extremes, the combinations of compression and bending are infinitely variable, explaining why no unique critical load exists for inelastic buckling.

3 Numerical analysis with Shanley-like column model

Although in practice engineers tend to use the over-conservative tangent-modulus theory to obtain simple and safe solutions to inelastic buckling problems, theoretically only Shanley's theory correctly describes the mechanics of the process. Shanley (1947) demonstrated his theory using a simplified column model consisting of two rigid legs and an elastic-plastic hinge composed of two axial elements. A modification of Shanley's model has been used as a basic model in this research.

3.1 *Geometry*

Shanley's model may be represented by a rigid cantilever supported by two identical "springs", as shown in Fig. 2. This is a direct analogue of the simple column of twice the length which is also shown in the figure. It has two degrees of freedom:

- Vertical movement u, which is the mean vertical movement of the two springs;
- Rotation θ, which is proportional to the difference in displacement of the springs.

Shanley's model is useful for general investigation of buckling, but is over-simplified for a rational numerical analysis of the problems addressed previously. Therefore, this basic model has been modified and extended as shown in Fig. 3.

Since inelastic buckling is significantly rate-related, two dampers, one vertical and one rotational, were added to the basic model. They respectively control the rates of change of the two degrees of freedom u and θ. They damp the

movement of the model in a controlled manner, which enables it to achieve the full buckling load-deflection equilibrium path rather than a sudden bifurcation when the column fails by buckling. In addition, by changing the values of the two damping coefficients the two extreme situations of inelastic buckling (bifurcation at the tangent-modulus or reduced-modulus loads) may be simulated.

The two-spring model was extended to a multi-spring model, representing the material continuity through the cross-section. The axial deformation of each spring is consistent with the linear strain-gradient assumption, and hence the mean and differential displacements of each pair of springs at the equivalent locations on either side of the central axis are still functions of the two DoFs u and θ. In this particular analysis the springs are all identical, having the same force-displacement curves and representing the same material, but the force level of each spring can differ from the others at any given time, depending on the global deformation and the force equilibrium of the column. For instance, some springs may already be in the plastic range when the others are still linear-elastic, and some may already have started unloading while others continue to load. A bilinear stress-strain curve with elastic strain reversal has been used in this analysis. Each spring characteristic can represent any material, either elastic or elasto-plastic, but the distribution of the spring displacements must remain linear.

In Shanley's mathematical analysis, the model is initially perfectly symmetric, with the load perfectly central. It is then assumed to start to rotate at the tangent-modulus buckling load, but the axial load continues to increase

thereafter. Shanley makes these assumptions because the purpose of his analysis is only to support his previous test results. However, for the purpose of this research, these assumptions have been considered as over-simplified and hence inappropriate. Without assuming the model to start to rotate at a certain load, the introduction of an initial imperfection as an arbitrary small rotation θ_0 was necessary to enable the analysis to guarantee numerical solutions. This also pre-defines the direction of deflection.

3.2 *Mathematical model*

Dynamic numerical analysis was conducted using a program based on the multi-spring model. The equations of motion were written for the static and dynamic forces and moments caused by the imposed load and reaction forces on the springs and dampers:

$$\Sigma F = 0: \qquad P = \sum_{i=1}^{2}\sum_{j=1}^{n} F_{sij} + F_{cv} \tag{4}$$

$$\Sigma M = 0: \qquad P\left(\theta_0 + \theta\right)L = \sum_{j=1}^{n} \frac{j}{n} \cdot \frac{B}{2}\left(F_{s2j-}F_{s1j}\right) + M_{cr} \tag{5}$$

The sign convention used in this analysis for the positive directions of force and moment is shown in Fig. 3.

The reaction force and moment applied to the two dampers derive from the velocities of the two DoFs:

$$F_{cv} = C_v \cdot \dot{u} \tag{6}$$

$$M_{cr} = C_r \cdot \dot{\theta} \tag{7}$$

Substituting Equations (6) and (7) into Equations (4) and (5) and rewriting:

$$\dot{u} = \left(P - \sum_{i=1}^{2} \sum_{j=1}^{n} F_{sij} \right) \Big/ C_v \tag{8}$$

$$\dot{\theta} = \left(P(\theta_0 + \theta) L - \frac{B}{2n} \sum_{j=1}^{n} j \cdot \left(F_{s2j} - F_{s1j} \right) \right) \Big/ C_r \tag{9}$$

According to the linear strain-gradient assumption the cross-section remains plane, and so the mean and differential displacements (and velocities) of each pair of springs at the equivalent locations on opposite sides are functions of u ($\dot{u}$) and θ ($\dot{\theta}$):

$$\left.\begin{aligned} u &= \frac{x_{1j} + x_{2j}}{2} \\ \theta &= \frac{x_{2j} - x_{1j}}{\frac{jB}{n}} \end{aligned}\right\} \quad \Rightarrow \quad \begin{cases} x_{1j} = u - \frac{jB}{2n}\theta \\ x_{2j} = u + \frac{jB}{2n}\theta \end{cases}$$

$$\left.\begin{aligned} \dot{u} &= \frac{\dot{x}_{1j} + \dot{x}_{2j}}{2} \\ \dot{\theta} &= \frac{\dot{x}_{2j} - \dot{x}_{1j}}{\frac{jB}{n}} \end{aligned}\right\} \quad \Rightarrow \quad \begin{cases} \dot{x}_{1j} = \dot{u} - \frac{jB}{2n}\dot{\theta} \\ \dot{x}_{2j} = \dot{u} + \frac{jB}{2n}\dot{\theta} \end{cases} \tag{10}$$

A bilinear force-deformation relationship, which allows elastic unloading, is applied to the springs in this preliminary stage (see Fig. 4). It may be written in the generalized form:

$$F_s = \alpha + \beta x \tag{11}$$

The formulation of α and β differs at various loading stages, as listed in Table 1. In the program, the loading stage of each spring is defined according to its deformation, velocity and force, all at the previous time step.

The tangent modulus k_t is defined to be 25% of the elastic modulus k. The proportional limit F_p of the bilinear force-deformation curve is defined as

$0.6P_t/2n$ to ensure that the springs become plastic before overall buckling of the model occurs in the inelastic range. The calculation of the theoretical tangent-modulus buckling load P_t is described in detail in Section 3.3.1.

A constant force is imposed on the model. This simulates the application of a gravity load on top of the column, in a single step but without impact, so that no initial velocity or acceleration is induced. In the initial time step, the unbalanced external and internal forces (whose difference is identical to the damping force) induce velocity, causing the model to move. The model continues to deform gradually through successive time steps until a new static equilibrium is reached, and this equilibrium position is recorded. The same procedure is repeated for successively higher loads, until the rotation of the model is seen to diverge, indicating its final failure by buckling. Plotting all the loads against the corresponding rotations θ recorded at equilibrium gives the full equilibrium path. Relaxation with explicit time integration is used for the numerical algorithm. The calculation procedure within each time step is illustrated in Fig. 5 and described below:

The two DoFs u_t and θ_t at time t may be calculated from their values $u_{t-\Delta t}$ and $\theta_{t-\Delta t}$ and their velocities $\dot{u}_{t-\Delta t}$ and $\dot{\theta}_{t-\Delta t}$ at the end of the previous time step, as they are assumed to increase linearly with time within each time increment Δt. The deformation of each spring x_t and its velocity at the end of the previous time step $\dot{x}_{t-\Delta t}$ are then calculated from u_t, θ_t, $\dot{u}_{t-\Delta t}$ and $\dot{\theta}_{t-\Delta t}$ by making use of the linear strain-gradient assumption (Eq. (10)). The loading stage of the spring on the force-deformation curve (Fig. 4) is then detected

according to its force $F_{s,t-\Delta t}$, deformation $x_{t-\Delta t}$ and velocity $\dot{x}_{t-\Delta t}$ at the end of the previous time step. Unloading is detected when the spring velocity $\dot{x}$ is seen to alter from positive to negative, and the corresponding force F_{UL} and deformation x_{UL} are recorded. The coefficients α_t and β_t are then calculated for the current loading stage, from the corresponding formulae in Table 1, which enables the spring-force F_s to be determined from Eq. (11). The same procedure is repeated for all of the springs. Finally, the velocities of the two DoFs $\dot{u}_t$ and $\dot{\theta}_t$ are calculated from Equations (8) and (9) for use in the next time step.

3.3 *Calculation of theoretical buckling loads*

As mentioned in Section 2, the tangent-modulus and reduced-modulus loads should respectively be the lower and upper boundaries of the buckling load path of a column, as shown in Fig. 1, and therefore they are used to validate the results of the numerical analysis on the Shanley-like model. The calculation of these two theoretical buckling loads of the multiple-spring model according to the corresponding theories has been programmed and is described in this section.

3.3.1 *Calculation of tangent-modulus buckling load* P_t

In the tangent-modulus theory, the column is assumed to remain straight and in stable equilibrium until the tangent-modulus critical buckling load P_t is reached. At $P = P_t$, the column is in neutral equilibrium in either the straight, or an arbitrary slightly deflected, position. Beyond this critical load, the

column will lose its stability and collapse by buckling under the slightest disturbance. In accordance with this theory, the tangent-modulus load P_t of the multiple-spring model is calculated. When the applied load reaches P_t, the model suddenly bifurcates from its vertical static equilibrium position to a deflected static equilibrium position, by means of a small rotation $\tilde{\theta}$ whilst the load remains constant, as shown in Fig. 6. It should be noted that, since no dynamic aspect is involved here, the dampers are excluded. The moment equilibrium equations of the model at these two possible equilibrium positions are written as:

When vertical: $\sum M = 0$

So that
$$\begin{aligned} 0 = &\left(F_{s21} - F_{s11}\right)\cdot\frac{B/2}{n}\cdot 1 \\ &+\left(F_{s22} - F_{s12}\right)\cdot\frac{B/2}{n}\cdot 2 \\ &\vdots \\ &+\left(F_{s2j} - F_{s1j}\right)\cdot\frac{B/2}{n}\cdot j \\ &\vdots \\ &+\left(F_{s2n} - F_{s1n}\right)\cdot\frac{B/2}{n}\cdot n \end{aligned}$$

or
$$0 = \sum_{j=1}^{n}\left(F_{s2j} - F_{s1j}\right)\cdot\frac{Bj}{2n} \qquad (12)$$

When deflected to $\tilde{\theta}$: $\sum M = 0$

So that
$$P_t\tilde{\theta}L = \left(F_{s21} - F_{s11}\right)\cdot\frac{B/2}{n}\cdot 1 + \left(\Delta F_{s21} - \Delta F_{s11}\right)\cdot\frac{B/2}{n}\cdot 1$$
$$+\left(F_{s22} - F_{s12}\right)\cdot\frac{B/2}{n}\cdot 2 + \left(\Delta F_{s22} - \Delta F_{s12}\right)\cdot\frac{B/2}{n}\cdot 2$$
$$\vdots$$
$$+\left(F_{s2j} - F_{s1j}\right)\cdot\frac{B/2}{n}\cdot j + \left(\Delta F_{s2j} - \Delta F_{s1j}\right)\cdot\frac{B/2}{n}\cdot j$$
$$\vdots$$
$$+\left(F_{s2n} - F_{s1n}\right)\cdot\frac{B/2}{n}\cdot n + \left(\Delta F_{s2n} - \Delta F_{s1n}\right)\cdot\frac{B/2}{n}\cdot n$$

or
$$P_t\tilde{\theta}L = \sum_{j=1}^{n}\left(F_{s2j} - F_{s1j}\right)\cdot\frac{Bj}{2n} + \sum_{j=1}^{n}\left(\Delta F_{s2j} - \Delta F_{s1j}\right)\cdot\frac{Bj}{2n} \qquad (13)$$

Substituting Eq. (12) into (13) gives:

$$P_t\tilde{\theta}L = \sum_{j=1}^{n}\left(\Delta F_{s2j} - \Delta F_{s1j}\right)\cdot\frac{Bj}{2n} \qquad (14)$$

When the column is straight at $P = P_t$, the applied force P_t is uniformly distributed among all the springs, and so the reaction force on each spring is identical and equal to $P_t/2n$; the spring stiffnesses at this stage are all equal. They are in fact the tangent modulus k_t of the force-deformation curve of each at the corresponding force value in the plastic stage; this will be referred to as k_1. When the model starts to rotate at this load, then since the rotation occurs from the straight position and is very small, it is assumed that no strain reversal takes place in the springs on the left-hand side of Fig. 6. It is also assumed that the stiffnesses of the springs remain the same, although for a nonlinear force-displacement curve they should change as a group and vary slightly from one another due to the contribution of the additional spring forces ΔF_s resulting from the rotation. Since a bilinear force-deformation relationship,

as shown in Fig. 4, applies to the springs, the tangent modulus k_t is uniquely defined, and so the additional spring forces ΔF_s resulting from the rotation are given by

$$\Delta F_{sij} = k_t \Delta x_{ij} \tag{15}$$

Substituting Eq. (15) into (14) gives

$$P_t \tilde{\theta} L = \sum_{j=1}^{n} k_t \left(\Delta x_{2j} - \Delta x_{1j} \right) \cdot \frac{Bj}{2n} \tag{16}$$

Since the deformations of the springs should vary linearly across the cross-section in order to fulfil the assumption that plane cross-sections remain plane, the rotation $\tilde{\theta}$ has the following relationship with the resulting additional deformations of the springs:

$$\tilde{\theta} = \frac{\Delta x_{2j} - \Delta x_{1j}}{\frac{B}{n} \cdot j} \tag{17}$$

Substituting Eq. (17) into (16) gives

$$P_t \tilde{\theta} L = \sum_{j=1}^{n} k_t \left(\tilde{\theta} \cdot \frac{B}{n} \cdot j \right) \cdot \frac{Bj}{2n} \; = \frac{k_t B^2 \tilde{\theta}}{2n^2} \; \sum_{j=1}^{n} j^2 \tag{18}$$

Eq. (18) has two unknowns $\tilde{\theta}$ and P_t, and the two solutions are:

$$\begin{cases} \tilde{\theta} = 0 & \text{(i)} \\ P_t = \dfrac{k_t B^2}{2L} \; \dfrac{\sum_{j=1}^{n} j^2}{n^2} & \text{(ii)} \end{cases} \tag{19}$$

Solution (i) implies that, as long as the column remains straight, it is always in equilibrium under any load. Solution (ii) gives the value of the tangent-

modulus critical buckling load, under which the column is in equilibrium with a deflected shape for which $\tilde{\theta} \neq 0$.

It should be noted that the use of the bilinear force-deformation relationship (Fig. 4) simplifies this calculation due to the uniqueness of k_t, whilst when the nonlinear curve is used an iterative procedure is needed to determine the value of k_t. This procedure involves, firstly, estimating the value of P_t. This trial value, say P_1, is a little larger than the proportional limit. Then uniformly divide P_1 between the springs, allocating F_{s1} to each. The tangent modulus k_t is then determined from the force-deformation curve, as the gradient at F_{s1}. Substituting k_t into Eq. (19), a second estimate of P_t, say P_2, is made. If P_2 is close enough to P_1, then it is accepted to be the tangent-modulus buckling load; otherwise, this iteration needs to be repeated until an acceptable agreement between P_1 and P_2 is obtained.

3.3.2 *Calculation of reduced-modulus buckling load* P_r

It should be noted that calculation of the tangent-modulus buckling load is solely based on the moment equilibrium of the model; its force equilibrium is not checked. Since unloading of springs on the left-hand side of Fig. 6 is ignored, the incremental reaction forces of the springs ΔF_{sij} are all compressive, which results in an increase in the sum of the spring forces whilst the applied load is assumed to remain constant. In this case the model will fail to maintain its force equilibrium. The reduced-modulus theory attempts to mitigate this contradiction of the tangent-modulus theory by taking into

account the unloading on the concave side of the column whilst still assuming that the column fails by buckling at a constant critical load, at the so-called reduced-modulus buckling load P_r. The vertical and deflected equilibrium positions at this critical load are illustrated in Fig. 7. The force and moment equilibrium equations of the model in these two equilibrium positions can be stated as

$$\sum F = 0 \qquad \Rightarrow \qquad \sum \Delta F_{sij} = 0 \tag{20}$$

$$\sum M = 0 \qquad \Rightarrow \qquad P_r \tilde{\theta} L = \sum_{j=1}^{n} \left(\Delta F_{s2j} - \Delta F_{s1j} \right) \cdot \frac{Bj}{2n} \tag{21}$$

However, the additional deformation Δx_{ij} and force ΔF_s may be negative (compression is positive) for those springs which unload. Therefore, it is essential to determine the position of the axis of rotation in order to find out which springs unload whilst the others continue to load. An iterative procedure is needed: firstly, estimate the value of the distance a between the neutral axis and the centre-line of the model. This estimate should start from the half model-width $B/2$ and then decrease towards zero. Since the deformations of the springs distribute linearly across the cross-section, they can be determined as long as a is known.

$$\Delta x_{ij} = f(a) \cdot \tilde{\theta} \tag{22}$$

Depending on their relative position to the neutral axis, the spring force increments ΔF_s are:

$$\begin{aligned} &\text{For the springs to the left of the rotation axis:} \quad \Delta F_{sij} = k \Delta x_{ij} \\ &\text{For the springs to the right of the rotation axis:} \quad \Delta F_{sij} = k_t \Delta x_{ij} \end{aligned} \tag{23}$$

Substituting Eq. (22) into (23) gives:

$$\begin{aligned} &\text{For the springs to the left of the rotation axis:} \quad \Delta F_{sij} = kf\left(a\right)\cdot\tilde{\theta} \\ &\text{For the springs to the right of the rotation axis:} \quad \Delta F_{sij} = k_t f\left(a\right)\cdot\tilde{\theta} \end{aligned} \tag{24}$$

The additional forces ΔF_s on all the springs are summed. If Eq. (20) is satisfied, then the estimate of a is accepted; otherwise, this iteration needs to be repeated. After the position of the axis of rotation has been determined, substituting the value of ΔF_s back into Eq. (21) and eliminating $\tilde{\theta}$ from both sides of the equation finally gives the value of the reduced-modulus buckling load P_r.

4 Results & discussion

4.1 *An example model*

The results of the numerical analyses on the Shanley-like model are presented in Figures 8-17. It should be noted that the results presented in this section are all taken from a single example with the specifications listed in Table 2. The tangent-modulus and reduced-modulus critical buckling loads of this particular model are 96.25 N and 169.5 N, respectively. The position of the axis of rotation needed for calculation of the reduced-modulus buckling load lies between the 3rd and 4th springs on the left-hand side of Fig. 7, with a = 1.8 mm.

Figures 8(a)-(h) to 15(a)-(h) plot selected structural responses of the model under the following applied loads: (a) 70 N, (b) 96.25 N (P_t), (c) 97 N, (d) 98 N, (e) 160 N, (f) 169 N, (g) 169.5 N (P_r) and (h) 170 N. Fig. 8 shows the

development with time of the resultant of the reaction forces on all the springs ΣF_{sij}, the reaction force at the vertical damper F_{cv}, and the reaction moment at the rotational damper M_{cr}, under the constant applied load P. Figures 9-12 illustrate the development of the two DoFs u and θ and their velocities $\dot{u}$ and $\dot{\theta}$ during the same period of time. The deformation x_{ij} and velocity $\dot{x}_{ij}$ of each spring, and their force-deformation relationship $F_{sij} - x_{ij}$ during the same period are respectively shown in Figures 13-15.

The grey straight lines in Fig. 8 illustrate the constant loading imposed on the model. According to Eq. (4), the static external force P should be balanced by the dynamic internal forces F_{sij} and F_{cv}. In the initial step, the reaction forces F_{sij} on the springs are zero, so algebraically F_{cv} must be identical to P in order to maintain the equilibrium of the model. This physically induces a velocity ($\dot{u}$) to the model and initiates its vertical movement u. This corresponds to the initial increase from zero of u, shown in Fig. 9, and the large initial value of $\dot{u}$ in Fig. 10 in all the loading cases.

Compared to the rapid initial increase in u, the initial velocity of the rotation $\dot{\theta}$ is very modest, undergoing a gradual increases and reaching a peak value, as shown in Fig. 12. This can easily be explained by Eq. (5), according to which the initial value of $\dot{\theta}$ should be equal to $P\theta_0 L/C_r$, whose value is limited by the very small magnitude of the initial imperfection θ_0.

When subject to any load smaller than the reduced-modulus buckling load P_r, the motion of the model always stabilises after a certain period of time,

depending on the magnitude of the applied force. As shown in Fig. 8, the total spring force ΣF_{sij} approaches the applied force P, whilst the reaction force F_{cv} on the vertical damper eventually returns to zero. This corresponds to the stabilisation of u, θ and x_{ij} shown in Figures 9, 11 and 13. The vanishing of $\dot{u}$ and $\dot{\theta}$ has been used to indicate static equilibrium of the model in the numerical modelling. However, when the applied load is equal to or larger than P_r, the model is no longer able to re-establish static equilibrium at all. It is seen in Figures 9-15 (g) and (h) that the movement of the model continues at a constant rate at $P = P_r$ and even diverges at an increasing rate when $P > P_r$, which indicates a loss of stability. Correspondingly, it is seen that the total spring force ΣF_{sij} never reaches the applied force P, whilst F_{cv} and M_{cv} either reach a constant value or increase indefinitely at a growing rate in Figures 8(g) and 8(h). This indicates that the reduced-modulus buckling load P_r is the asymptotic upper limit of the loads under which a perfectly-straight simply-supported column is able to achieve a deformed static equilibrium state.

Checking all the applied forces P which enable re-stabilisation of the model (those which are smaller than P_r as mentioned above), with the amount of rotation θ that they induce at the re-stabilisation, as illustrated for a few example cases in Fig. 11, it is found that the amount of rotation induced by the forces that are smaller than the tangent-modulus buckling load P_t is very small, but it starts to increase significantly as soon as P increases beyond P_t.

Considering that a very small initial imperfection has been applied, this behaviour is consistent with Shanley's statement that an initially straight and centrally loaded column will remain straight below P_t and bending will begin as soon as P_t is exceeded.

When the applied force and its consequent rotation are sufficiently large, differences between the deformations x_{ij} of the springs, and between their velocities $\dot{x}_{ij}$, are observed, and some of the springs on the left-hand side of Fig. 3 start to unload. For example, considering Figures 13(e) and 14(e), initially the compressive deformations of the springs all increase almost identically from zero, indicating that very little rotation occurs, and the springs are compressed almost uniformly. At about one second, the deformations and velocities of the springs start to vary more markedly. As the model starts to rotate, the deformations of the springs on the right-hand side of Fig. 3 (the thin lines) continue to increase rapidly (corresponding to the increase in their velocities in Fig. 14(e)). The deformations of the springs on the left-hand side of Fig. 3 (the thick lines) increase at lower rates, some even starting to decrease with their velocities becoming negative, as shown in Fig. 14(e)). In addition, due to the linear strain-gradient assumption the differential deformation of the pair of springs at the column edges is larger than that of the pair nearest to the centre for a certain global angle of rotation θ. Finally, the movement of the model gradually stabilizes and the deformation of each spring reaches a constant value. It is seen in Fig. 15(e) that, because almost no rotation occurs initially, the forces and deformations of the springs are nearly identical, and are shown as the single line from zero to point A. Soon

after the model starts to rotate, some of the springs on the left-hand side of Fig. 3 start to unload, while the others continue to load.

It should be noted especially that when the applied force P is equal to the tangent-modulus buckling load P_t, the buckling behaviour of the model is distinct from its behaviour when loaded with either larger or smaller loads. It is seen in Figures 11(b) and 12(b) that initially θ increases at a constant rate, and then $\dot{\theta}$ rapidly drops to zero as the model achieves a new static equilibrium with a deformed shape. This re-stabilisation process takes significantly longer than when the model is less loaded. It is interesting to note that this linear increase of θ at constant $\dot{\theta}$ occurs in no other loading cases except when the applied load is identical to the reduced-modulus buckling load.

4.2 *Effects of relative damping and initial imperfection*

A normalised relative damping ratio R_d is introduced to represent the relationship between the vertical and rotational damping. Assuming the vertical and rotational dampers are the product of a continuous damping layer which is uniformly distributed across the model base and has a damping coefficient $\tilde{c}$, the damping reaction force and moment imposed by the vertical and rotational damping are:

$$F_{cv} = \int_0^B \dot{u}\ \tilde{c} dx = \dot{u}\ B\ \tilde{c} = C_v\ \dot{u} \tag{25}$$

$$M_{cr} = \int_{-B/2}^{B/2} \left(\dot{\theta}\ x + \dot{u}\right) x\ \tilde{c}\ dx = \dot{\theta}\ \frac{B^3}{12}\ \tilde{c} = C_r\ \dot{\theta} \tag{26}$$

Hence, R_d is defined as $\frac{C_r}{B^2 C_v}$.

Plotting all the applied loads P which enable the model to re-stabilise (those which are smaller than P_r) against the corresponding rotations θ, recorded at static equilibrium, gives the buckling load-rotation path of the model. Fig. 16(a) shows the buckling load-rotation paths of models for various values of R_d. Fig. 16(b) is a magnification of the framed part of Fig. 16(a). These are then validated against the theoretical tangent-modulus and reduced-modulus buckling loads (the short-dashed and long-dashed lines in Figures 16(a) and 16(b)). Irrespective of the variation of the damping, the rotation always starts to increase significantly at the tangent-modulus buckling load and then continues to increase as the force approaches the reduced-modulus buckling load, although the force never exceeds this upper bound (the model is never able to achieve a deformed static equilibrium state when the applied force is beyond P_r). The model therefore demonstrates inelastic buckling in the exact manner described by Shanley, irrespective of the magnitudes of damping.

The effects of damping have been investigated by varying R_d. Figures 16(a) and 16(b) show that with larger R_d, for example at R_d = 20E-2, the relatively large rotational damping results in a significant decrease of the amount of rotation which is induced by a certain applied load. It is not difficult to derive that as R_d tends to infinity the load-deflection curve will asymptotically approach to the reduced-modulus bifurcation line. However, it will never be exactly the same as the reduced-modulus bifurcation line since the model can

not remain perfectly vertical after P_t is exceeded. This is because, in order for the column load to go beyond P_t, the model must rotate, and so some of the springs unload. Otherwise the value of the tangent modulus k_t should be used for the entire cross-section, in which case, the column load cannot exceed P_t. On the other hand, as R_d decreases the rotation which is induced by a certain applied force increases, and hence the load-deflection curve moves towards the tangent-modulus bifurcation line. It is intuitive that a bifurcation failure at the tangent-modulus buckling load should be simulated when R_d approaches zero. However, as R_d decreases further, the approach of the load-deflection curve to the tangent-modulus bifurcation line ceases, and a convergence to a unique load-deflection curve is observed. This curve represents the static buckling load-deflection path at R_d = 0. The reason that the buckling load-deflection path does not asymptotically approach the tangent-modulus bifurcation line at R_d = 0 is that the column force P must increase beyond P_t to balance the additional spring forces which are induced by the rotation, soon after the model starts to rotate at $P = P_t$. This increase of P will continue as the rotation increases, in order to achieve further force equilibrium, until P approaches P_r. It is also seen in Fig. 16(b) that, for very small values of R_d, the load-deflection curve just beyond P_t experiences a change of curvature, showing an initial bifurcation at P_t which fails to continue due to the requirement of force equilibrium. It should also be noted that varying the absolute values of the two damping coefficients may change the

time scale of the dynamic process, but it does not affect its eventual static equilibrium as long as the ratio R_d remains the same.

The effect of initial imperfection has also been examined. Fig. 17 shows the buckling load paths of the model with various amount of initial imperfection. It can be seen that, as the initial imperfection increases, the load needed to induce a certain amount of rotation decreases, but the asymptotic upper limit to the loads under which the column is able to gain a deformed static equilibrium is still the reduced-modulus load P_r.

5 Conclusions

A simplified column model similar to Shanley's has been established, and its characteristics have been programmed for dynamic analysis. The mechanics of buckling in the inelastic range has been assessed using this model. An analysis which outputs the dynamic response of the model under static loading has been conducted. When subject to any load smaller than the reduced-modulus buckling load, the motion of the model always re-stabilises at a static equilibrium position with certain amount of rotation. Otherwise, when the applied force is equal or larger than the reduced-modulus load, failure due to instability occurs as the rotation continues to increase infinitely. When the applied force and its consequent rotation are sufficiently large, differences between the deformations of the springs and between their velocities are observed, and some of the springs on the less compressed side start to unload. The two cases in which the applied forces are respectively equal to the tangent-modulus and reduced-modulus buckling loads are similar in the respect that a linear increase of overall rotation is observed, although

the former achieves restabilisation whilst the latter finally loses stability. The static load-rotation path of the model is plotted from all the applied loads P which enable re-stabilisation of the model (those which are smaller than P_r) against their corresponding rotations θ, recorded at static equilibrium. Validation of the model against Shanley's inelastic buckling theory has been successful. Setting aside the very small initial imperfections applied, the model demonstrates that:

- An initially straight and centrally loaded column will remain straight below P_t
- As soon as P_t is exceeded, the column starts to bend and part of it is subject to strain reversal which enables the resultant column force to increase towards P_r
- The column resultant force increases simultaneously with rotation due to the requirement of force equilibrium
- The column force can not increase beyond P_r

The variation of damping does not affect the previous statements, but by varying the relative damping ratio R_d, the amount of rotation induced by a certain applied force alters accordingly, which causes the static buckling load-deflection path to move between the extremes:

- Very close to the reduced-modulus bifurcation line at $R_d = \infty$
- A unique curved path at $R_d = 0$

The effect of initial imperfection has also been examined. Increasing the initial imperfection causes the load which is needed to induce a certain amount of rotation to decrease, but it does not alter the asymptotic upper limit

to the loads under which the column is able to gain a deformed static equilibrium from the reduced-modulus buckling load.

ACKNOWLEDGMENT: *The principal author is grateful for the support of Corus Group Ltd and the Engineering and Physical Sciences Research Council of the United Kingdom, under a Dorothy Hodgkin Postgraduate Award.*

References

Anderberg, Y. and Thelanderson, S. (1976), *Stress and deformation characteristics of concrete at high temperatures. 2. Experimental investigation and material behaviour model*, Bulletin 54, Lund University, Sweden.

Bazant, Z. P. and Cedolin, L. (1991), *Stability of structures*, Oxford University Press, Oxford.

Bleich, F. (1952), *Buckling strength of metal structures*, McGraw-Hill, New York.

Considère, A. (1891), "Résistance des pièces comprimées", *In Congrès International des Procédés de Construction*, Libraire Polytechnique, Paris, **3**, 371.

Corona, E. (2001), "Stability of the Shanley column under cyclic loading", *Journal of Applied Mechanics*, **68**, 324-331.

Engesser, F. (1889), "Uber die knickfestigkeit gerader Stäbe*"*, *Zeischrift für Architektur und Ingenieurwesen*, **35** (4), 455-562.

European Committee for Standardization (2004)*, BS EN 1992: Eurocode 2: Design of concrete structures - Part 1-2: General rules - Structural fire design*.

Genna, F.and Symonds, P. S. (1987), "Induced vibrations and dynamic instabilities of a non linear structural model due to pulse loading", *Meccanica*, **22**, 144-149.

Gere, J. M. and Timoshenko, S. P. (1997), *Mechanics of materials; 4th edition.* PWS Publishing Company, Boston.

Khoury, G. A. (1996), *Performance of heated concrete - Mechanical properties*, Report to the Nuclear Installations Inspectorate of the Health and Safety Executive, London.

Khoury, G. A. (2006), "Strain of heated concrete during two thermal cycles. Part 1: Strain over two cycles, during first heating and at subsequent constant temperature", *Magazine of Concrete Research*, **58** (6), 367-385.

Khoury, G. A., Grainger, B. N. and Sullivan, P. J. E. (1985a), "Transient thermal strain of concrete: literature review, conditions within specimen and behaviour of individual constituents", *Magazine of Concrete Research*, **37** (132), 131-144.

Khoury, G. A., Grainger, B. N. and Sullivan, P. J. E. (1985b), "Strain of concrete during first heating to 600°C under load", *Magazine of Concrete Research*, **37** (133), 95-215.

Little, G. H. (2004), “The collapse of steel model columns with unequal flanges. I. Perfect”, *International Journal of Mechanical Sciences*, **46**, 1415-1436.

Massin, P., Triantafyllidis, N. and Leroy Y. M. (1999), “On the stability of strain-rate dependent solids. I – Structural examples”, *Journal of the Mechanics and Physics of Solids*, **47**, 1737-1779.

Schneider, U. and Horvath, J. (2003), *Behaviour of ordinary concrete at high temperatures*, Research reports of Vienna University of Technology, Vol. 9, Institute of Building Materials, Building Physics and Fire Protection, Vienna.

Shanley, F. R. (1947), “Inelastic column theory”, *Journal of the Aeronautical Sciences*, **14**(5), 261-268.

Figure Captions

Figure 1. Load-deflection curves given by various column buckling theories.

Figure 2. Shanley's model.

Figure 3. Multi-spring model.

Figure 4. Bilinear force-deformation relationship of the springs.

Figure 5. Calculation procedure within each time step of the numerical analysis with the Shanley-like model.

Figure 6. Sudden bifurcation from the vertical equilibrium position to a deflected equilibrium position at the tangent-modulus buckling load.

Figure 7. Sudden bifurcation from the vertical equilibrium position to a deflected equilibrium position at the reduced-modulus buckling load.

Figure 8. Development of the total reaction force on all the springs, the reaction force on the vertical damper and the reaction moment on the rotational damper over time under various applied loads.

Figure 9. Development of the vertical movement of the model over time under various applied loads.

Figure 10. Velocity of the vertical movement of the model.

Figure 11. Development of the rotation of the model over time under various applied loads.

Figure 12. Velocity of the rotation of the model.

Figure 13. Development of the deformation of each spring over time under various applied loads.

Figure 14. Velocity of the deformation of each spring.

Figure 15. Compressive load-deformation curves of the springs.

Figure 16. (a) Buckling load-rotation paths of the model with various damping ratios.

(b) Magnification of the framed section of Fig. 16(a).

Figure 17. Buckling load-rotation paths of the model with various initial imperfections.

Table Captions

Table 1. Formulation of α & β at various loading stages.

Table 2. Specification of the model analysed in Section 4.

Figure1

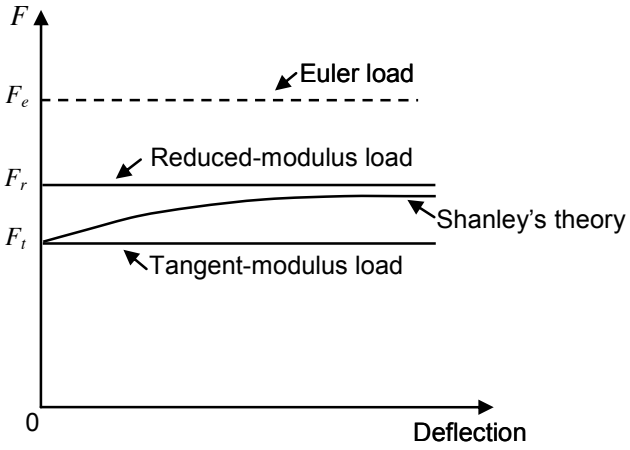
F
Euler load
F_e
Reduced-modulus load
F_r
Shanley's theory
F_t
Tangent-modulus load
0
Deflection

Figure2

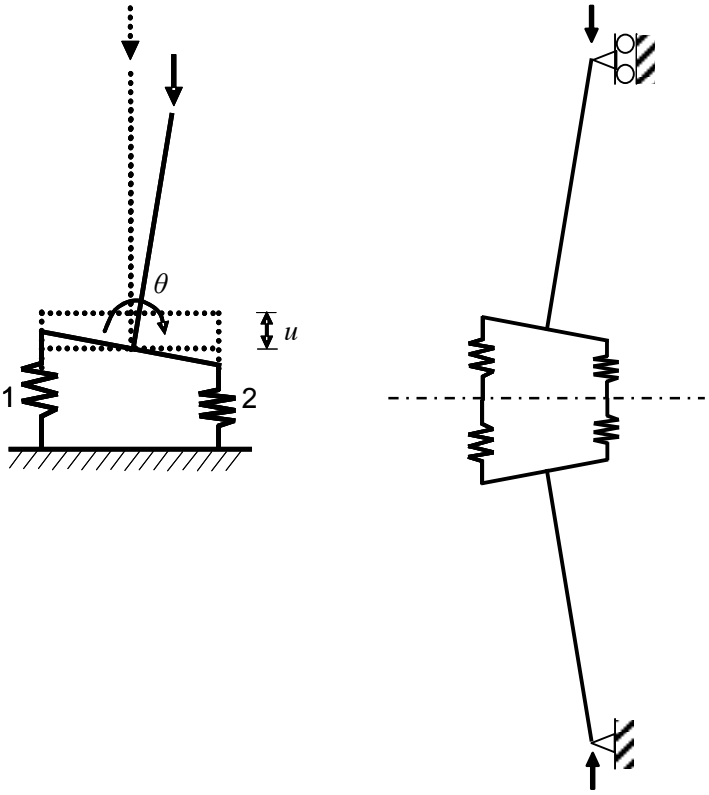

Figure3

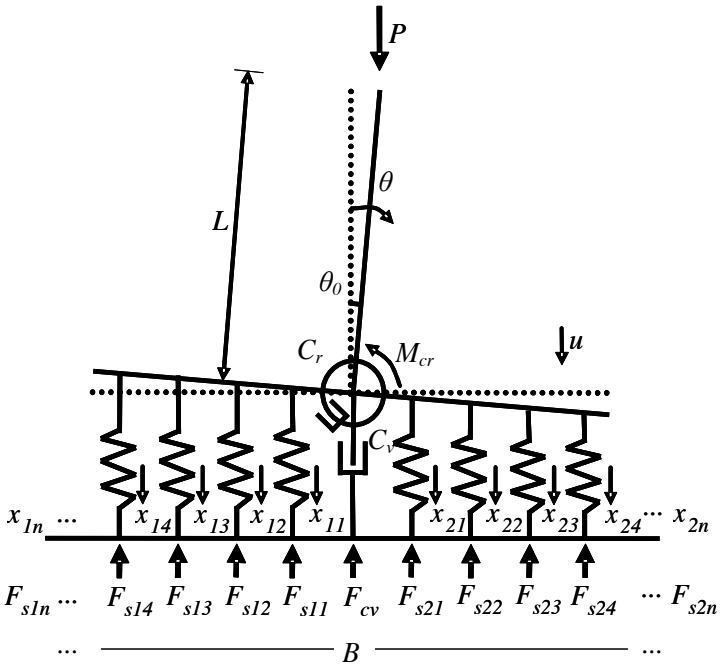
P
L
θ
θ0
Cr
Mcr
u
Cv
x1n ... x14 x13 x12 x11 x21 x22 x23 x24 ... x2n
Fs1n ... Fs14 Fs13 Fs12 Fs11 Fcv Fs21 Fs22 Fs23 Fs24 ... Fs2n
... B ...

Figure4

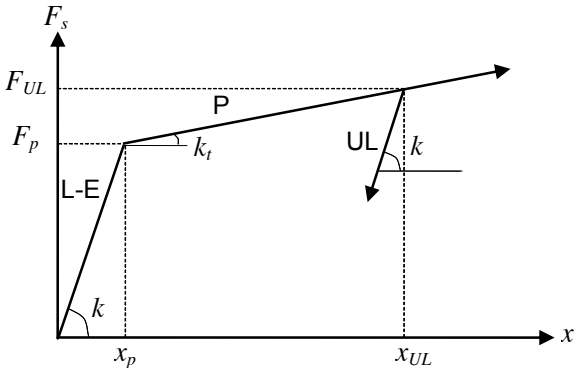

Figure5

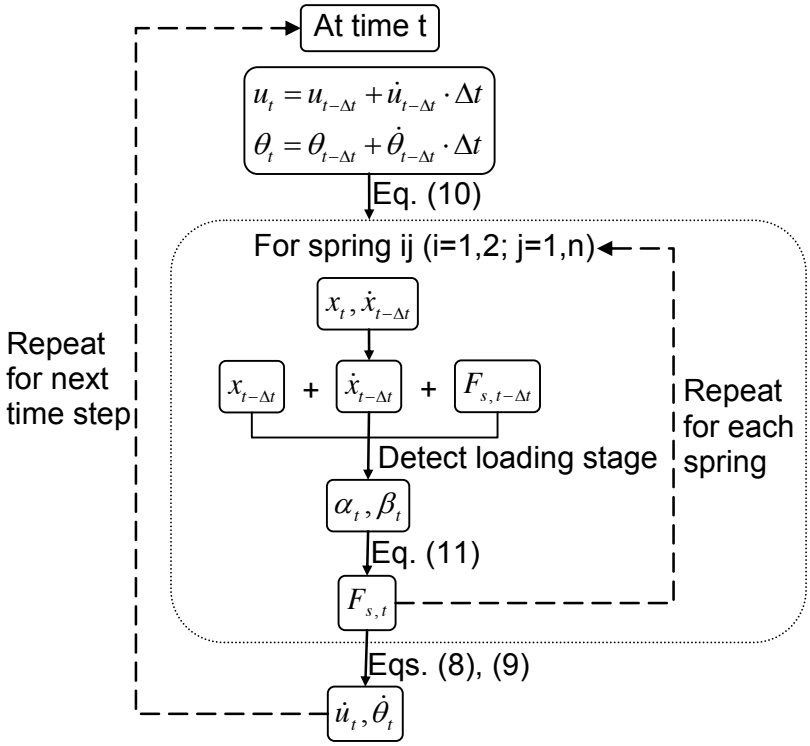
At time t
$u_t = u_{t-\Delta t} + \dot{u}_{t-\Delta t} \cdot \Delta t$
$\theta_t = \theta_{t-\Delta t} + \dot{\theta}_{t-\Delta t} \cdot \Delta t$
Eq. (10)
For spring ij (i=1,2; j=1,n)
$x_t, \dot{x}_{t-\Delta t}$
$x_{t-\Delta t}$ + $\dot{x}_{t-\Delta t}$ + $F_{s,t-\Delta t}$
Detect loading stage
α_t, β_t
Eq. (11)
$F_{s,t}$
Eqs. (8), (9)
$\dot{u}_t, \dot{\theta}_t$
Repeat for next time step
Repeat for each spring

Figure6

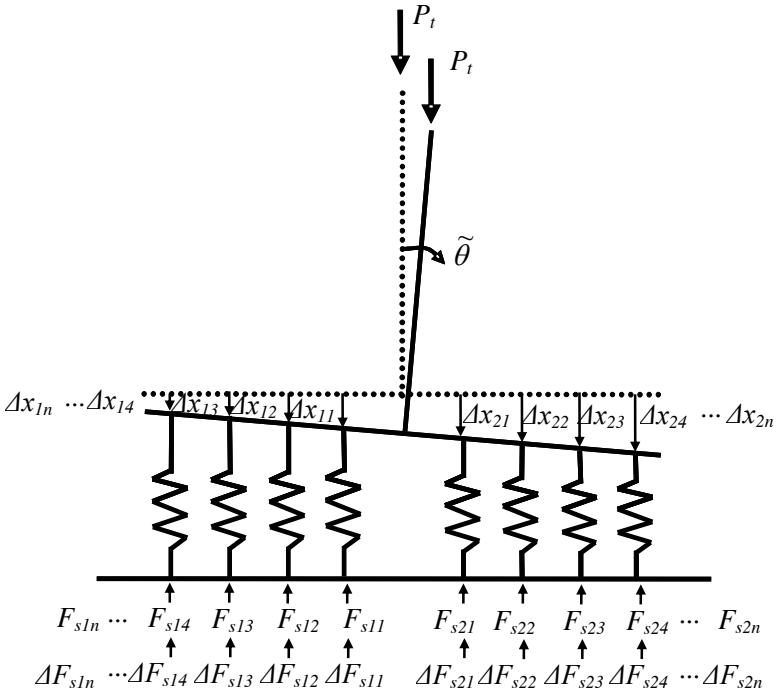
P_t
P_t
$\tilde{\theta}$
Δx_{1n} $\cdots\Delta x_{14}$ Δx_{13} Δx_{12} Δx_{11} Δx_{21} Δx_{22} Δx_{23} Δx_{24} $\cdots\Delta x_{2n}$
F_{s1n} $\cdots$ F_{s14} F_{s13} F_{s12} F_{s11} F_{s21} F_{s22} F_{s23} F_{s24} $\cdots$ F_{s2n}
ΔF_{s1n} $\cdots\Delta F_{s14}$ ΔF_{s13} ΔF_{s12} ΔF_{s11} ΔF_{s21} ΔF_{s22} ΔF_{s23} ΔF_{s24} $\cdots\Delta F_{s2n}$

Figure7

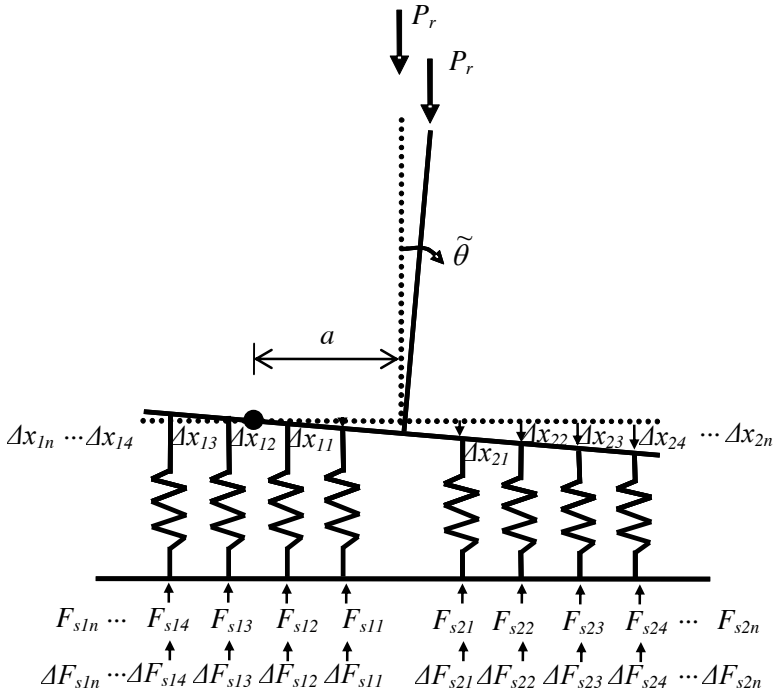
P_r
P_r
$\tilde{\theta}$
a
Δx_{1n} $\cdots \Delta x_{14}$ Δx_{13} Δx_{12} Δx_{11} Δx_{21} Δx_{22} Δx_{23} Δx_{24} $\cdots \Delta x_{2n}$
F_{s1n} $\cdots$ F_{s14} F_{s13} F_{s12} F_{s11} F_{s21} F_{s22} F_{s23} F_{s24} $\cdots$ F_{s2n}
ΔF_{s1n} $\cdots \Delta F_{s14}$ ΔF_{s13} ΔF_{s12} ΔF_{s11} ΔF_{s21} ΔF_{s22} ΔF_{s23} ΔF_{s24} $\cdots \Delta F_{s2n}$

Figure8

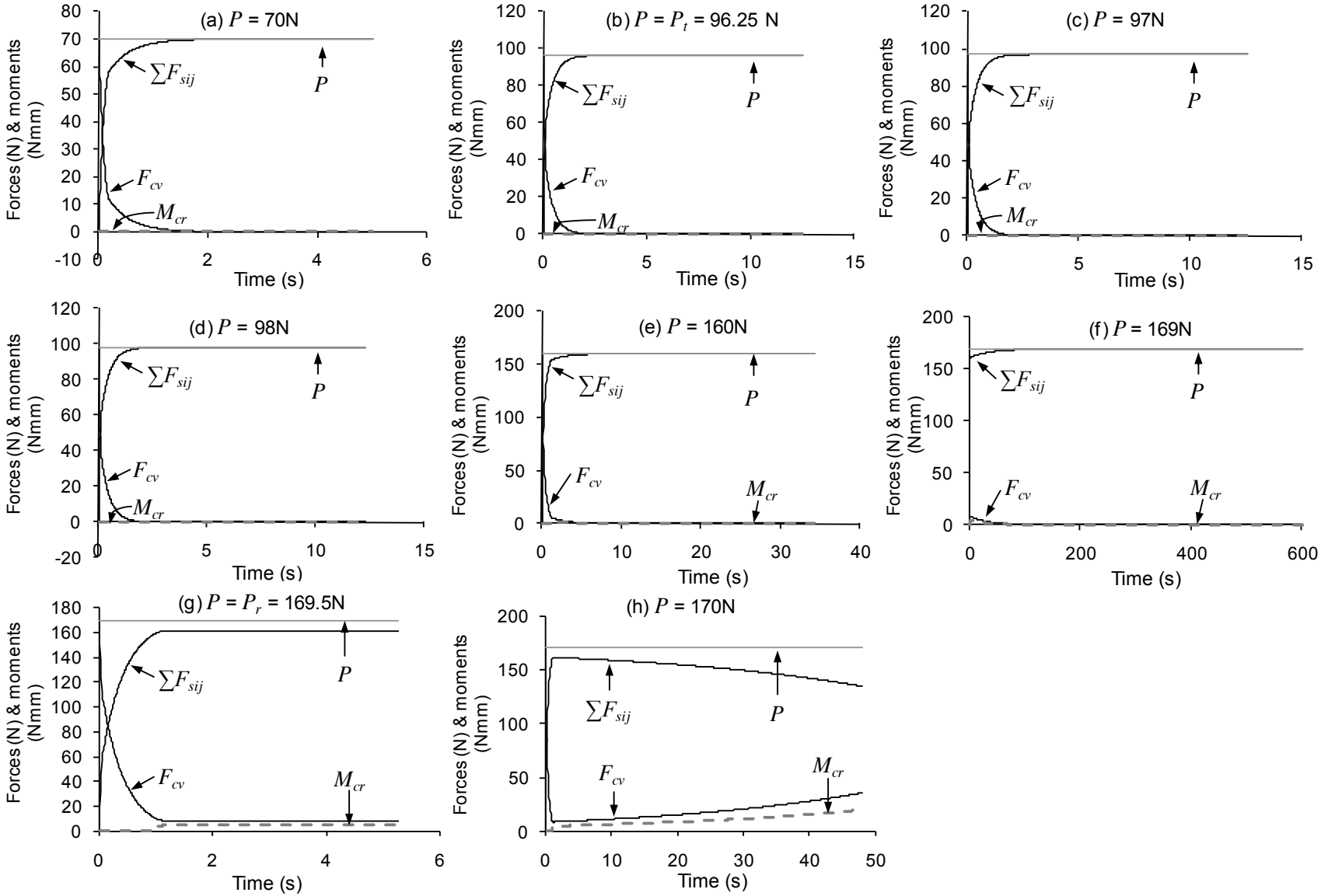
(a) P = 70N
(b) $P = P_t$ = 96.25 N
(c) P = 97N
(d) P = 98N
(e) P = 160N
(f) P = 169N
(g) $P = P_r$ = 169.5N
(h) P = 170N
Forces (N) & moments (Nmm)
Time (s)
$\sum F_{sij}$
P
F_{cv}
M_{cr}

Figure9

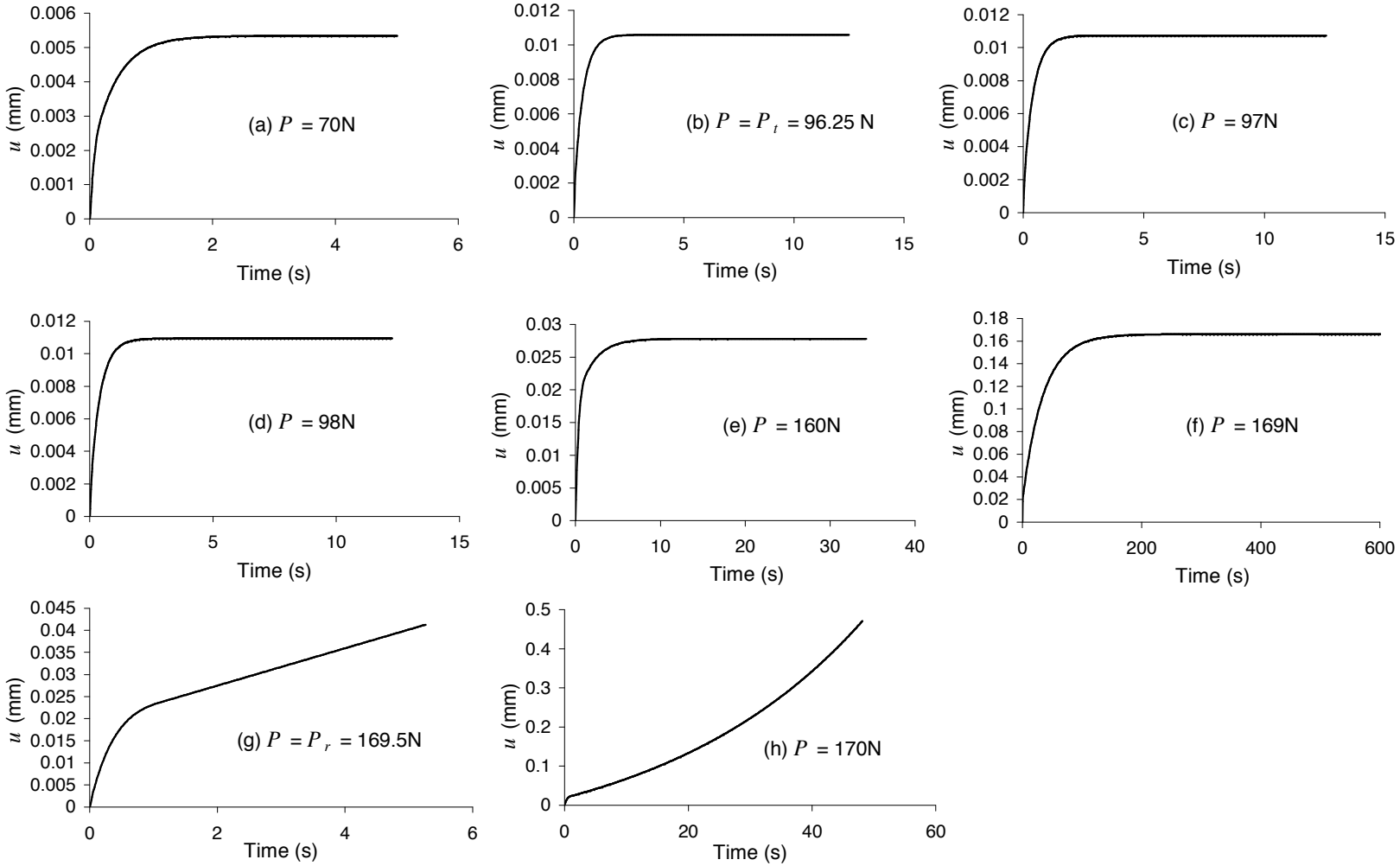
(a) P = 70N
(b) $P = P_t$ = 96.25 N
(c) P = 97N
(d) P = 98N
(e) P = 160N
(f) P = 169N
(g) $P = P_r$ = 169.5N
(h) P = 170N
u (mm)
Time (s)

Figure10

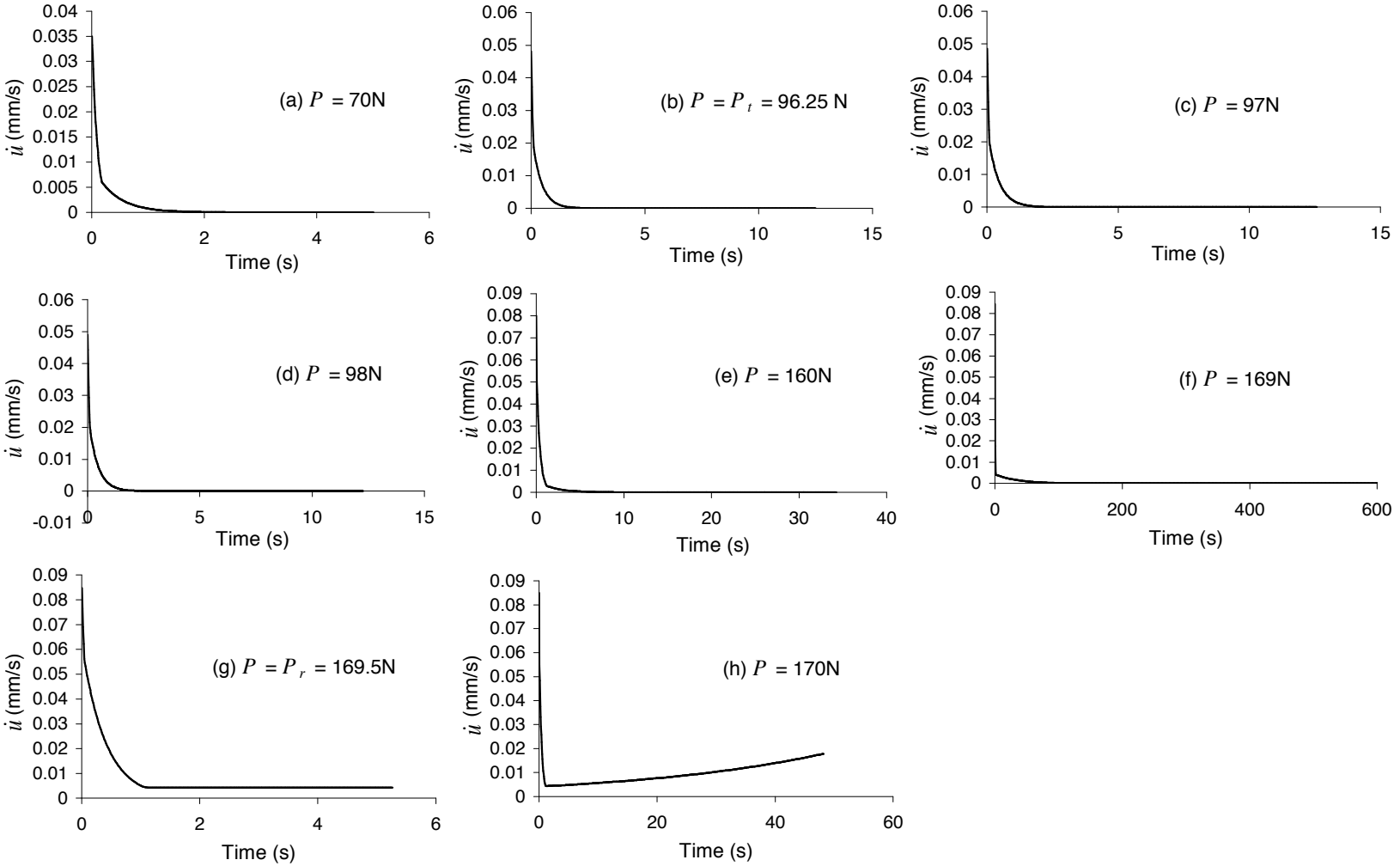
(a) P = 70N
(b) $P = P_t$ = 96.25 N
(c) P = 97N
(d) P = 98N
(e) P = 160N
(f) P = 169N
(g) $P = P_r$ = 169.5N
(h) P = 170N
$\dot{u}$ (mm/s)
Time (s)

Figure11

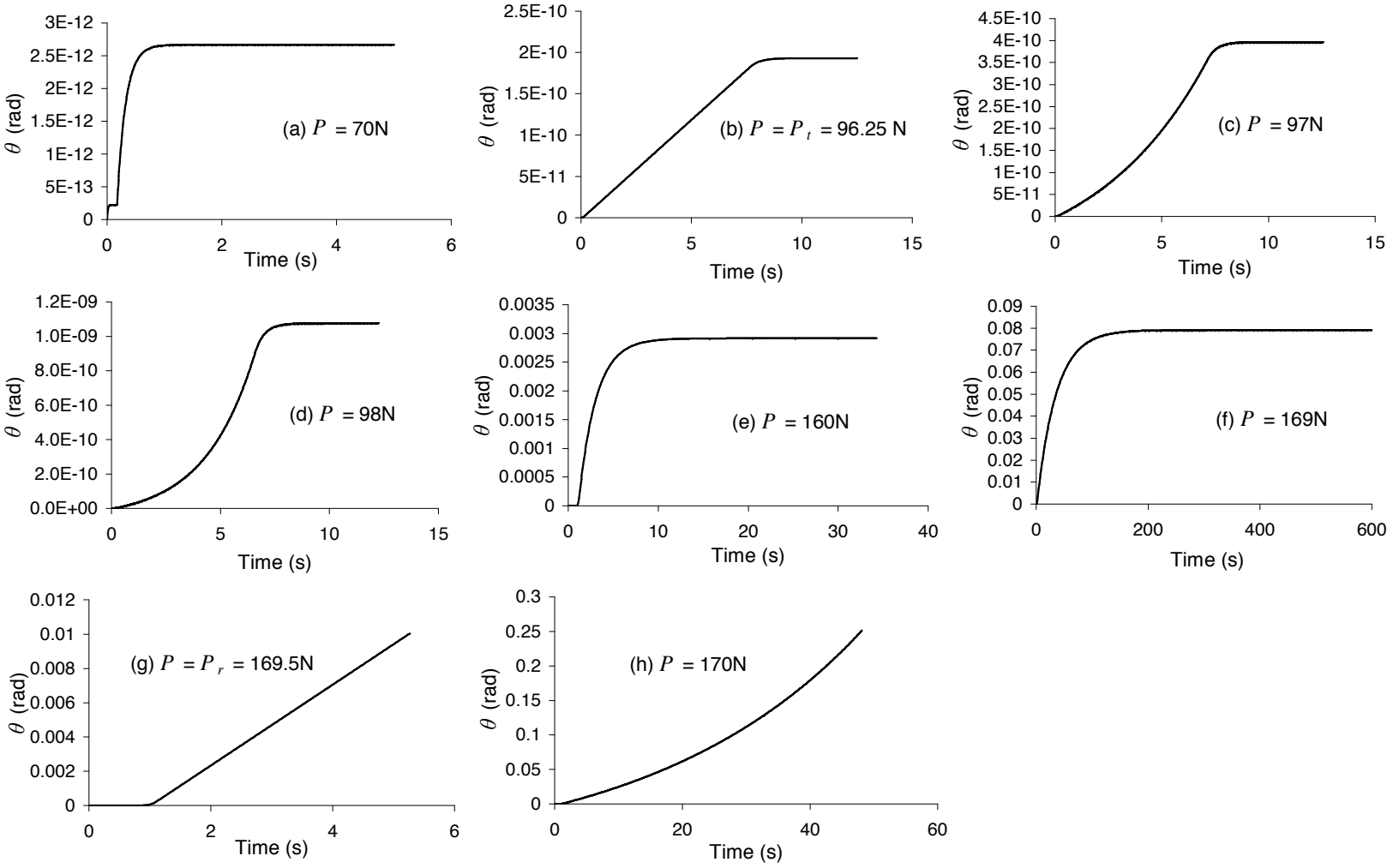
θ (rad)
Time (s)
(a) P = 70N
(b) P = P_t = 96.25 N
(c) P = 97N
(d) P = 98N
(e) P = 160N
(f) P = 169N
(g) P = P_r = 169.5N
(h) P = 170N

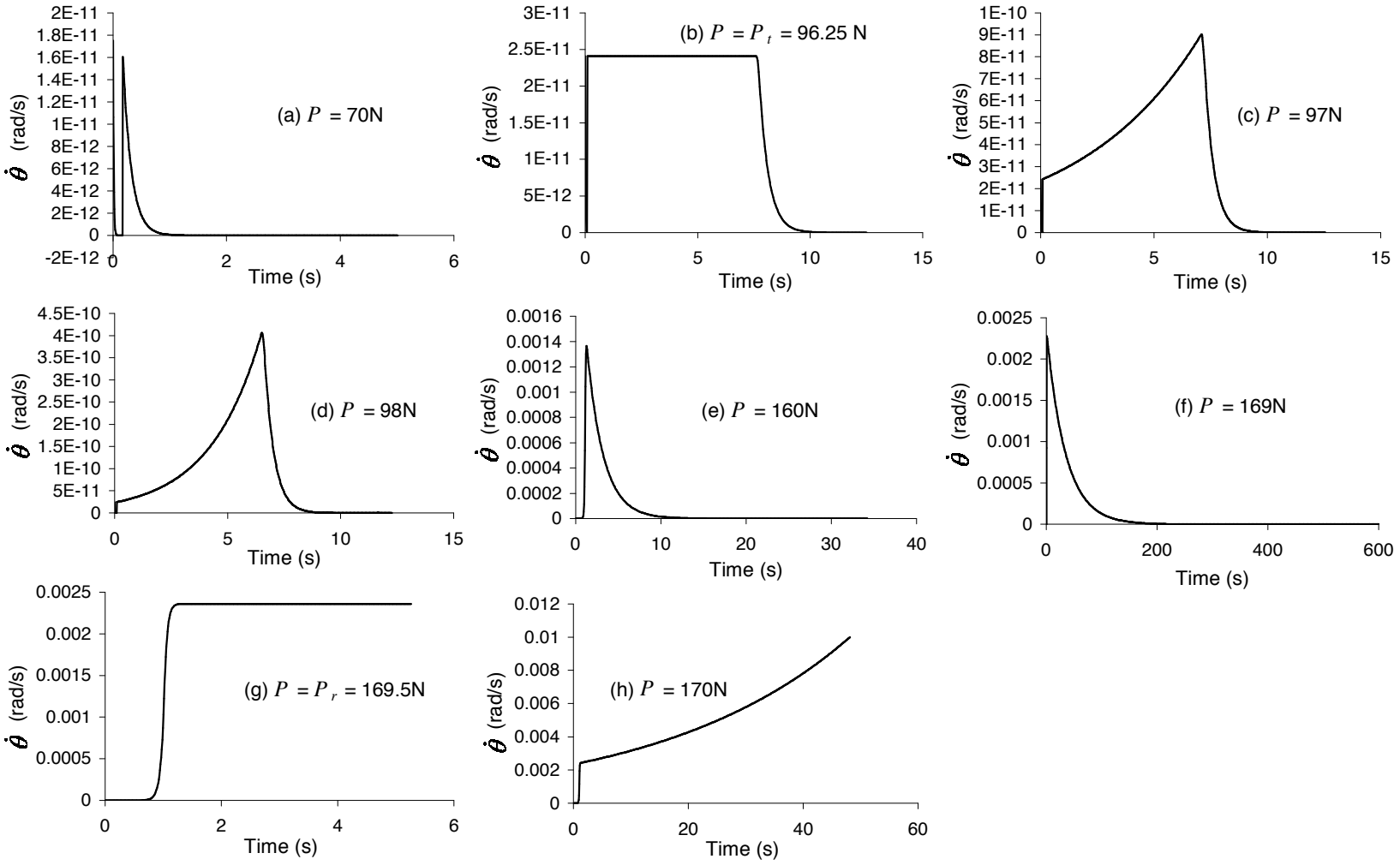
(a) P = 70N
(b) $P = P_t$ = 96.25 N
(c) P = 97N
(d) P = 98N
(e) P = 160N
(f) P = 169N
(g) $P = P_r$ = 169.5N
(h) P = 170N
$\dot{\theta}$ (rad/s)
Time (s)

Figure13

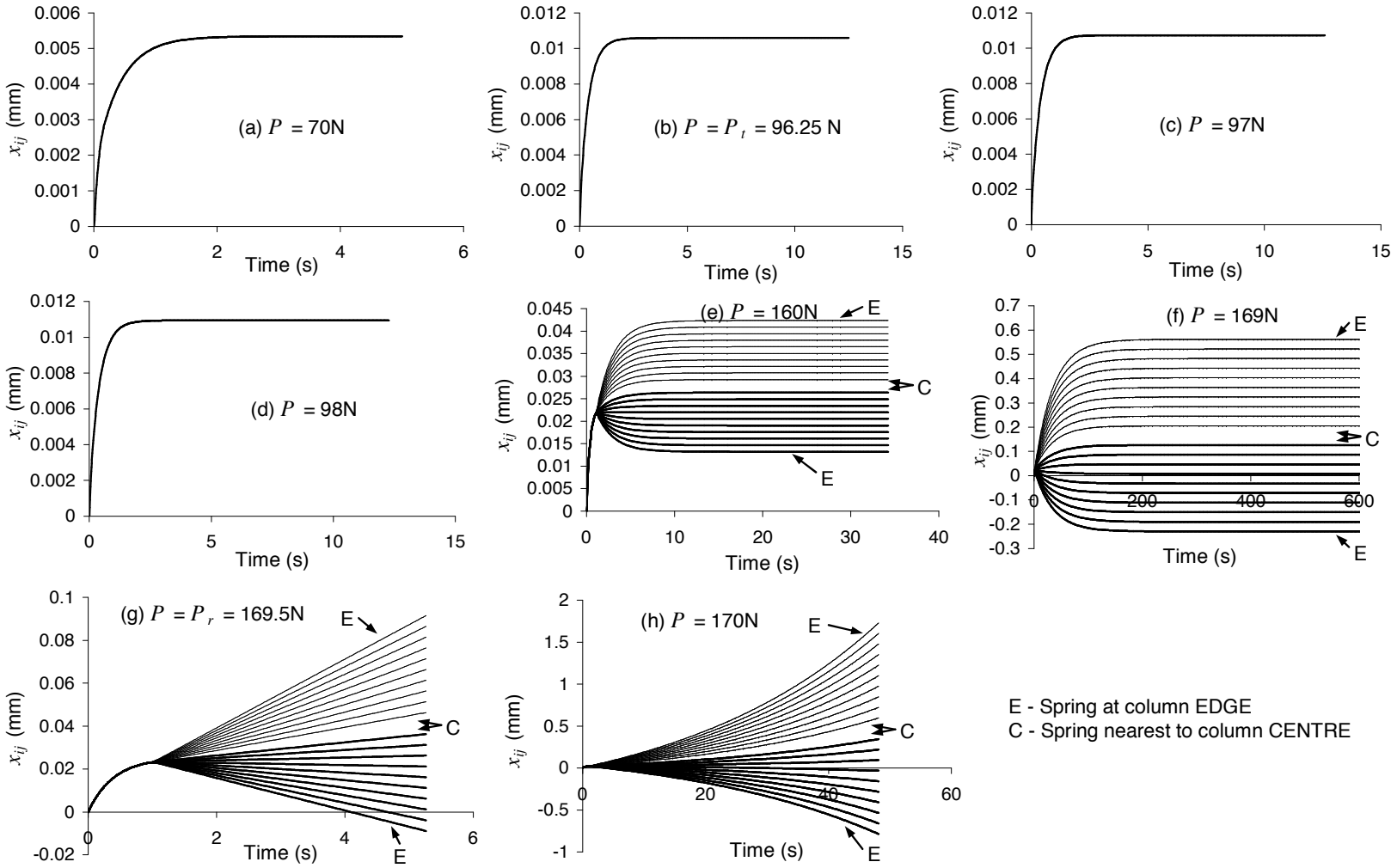
(a) P = 70N
(b) $P = P_t$ = 96.25 N
(c) P = 97N
(d) P = 98N
(e) P = 160N
(f) P = 169N
(g) $P = P_r$ = 169.5N
(h) P = 170N
x_{ij} (mm)
Time (s)
E
C
E - Spring at column EDGE
C - Spring nearest to column CENTRE

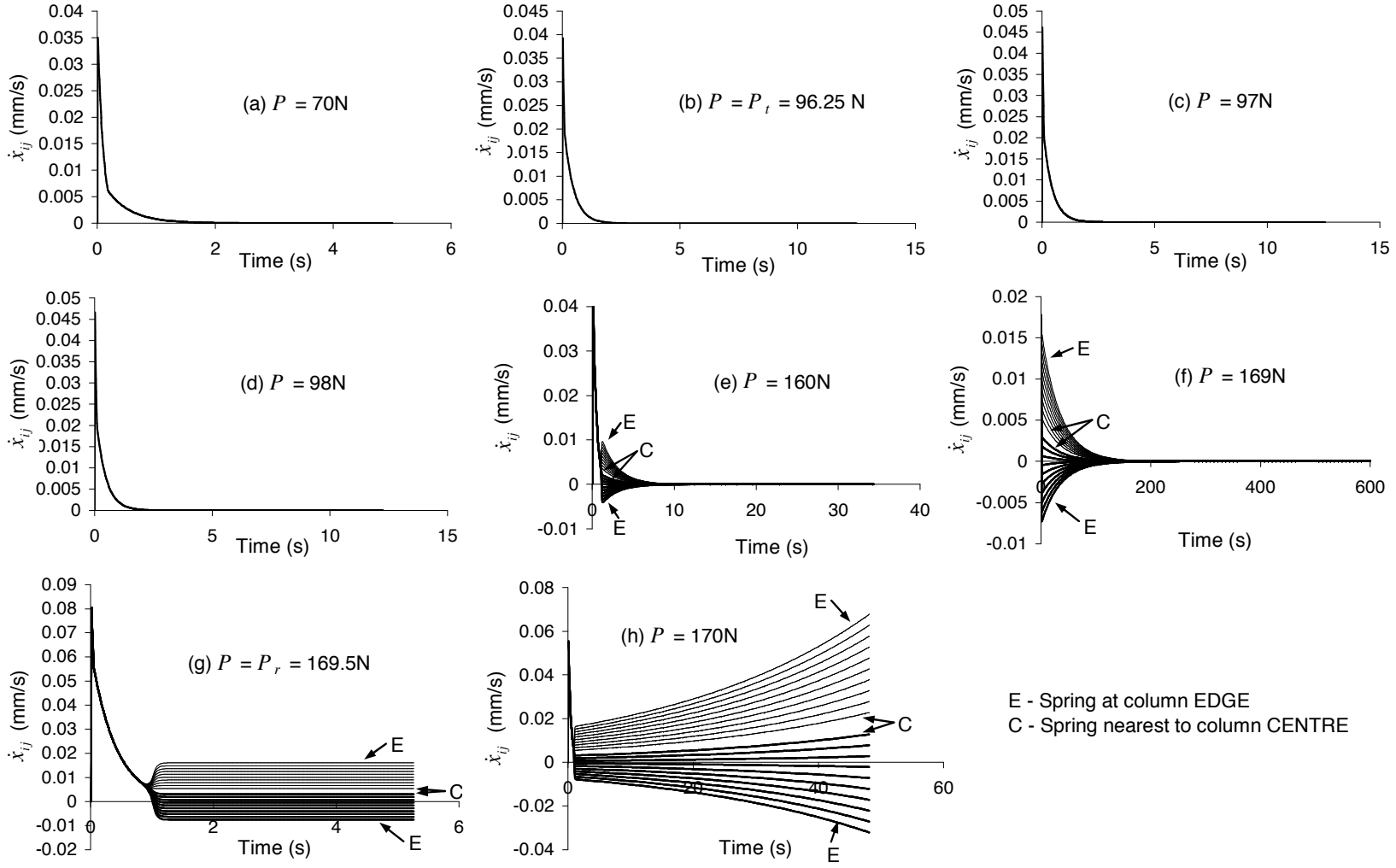
(a) P = 70N
(b) $P = P_t$ = 96.25 N
(c) P = 97N
(d) P = 98N
(e) P = 160N
(f) P = 169N
(g) $P = P_r$ = 169.5N
(h) P = 170N
$\dot{x}_{ij}$ (mm/s)
Time (s)
E
C
E - Spring at column EDGE
C - Spring nearest to column CENTRE

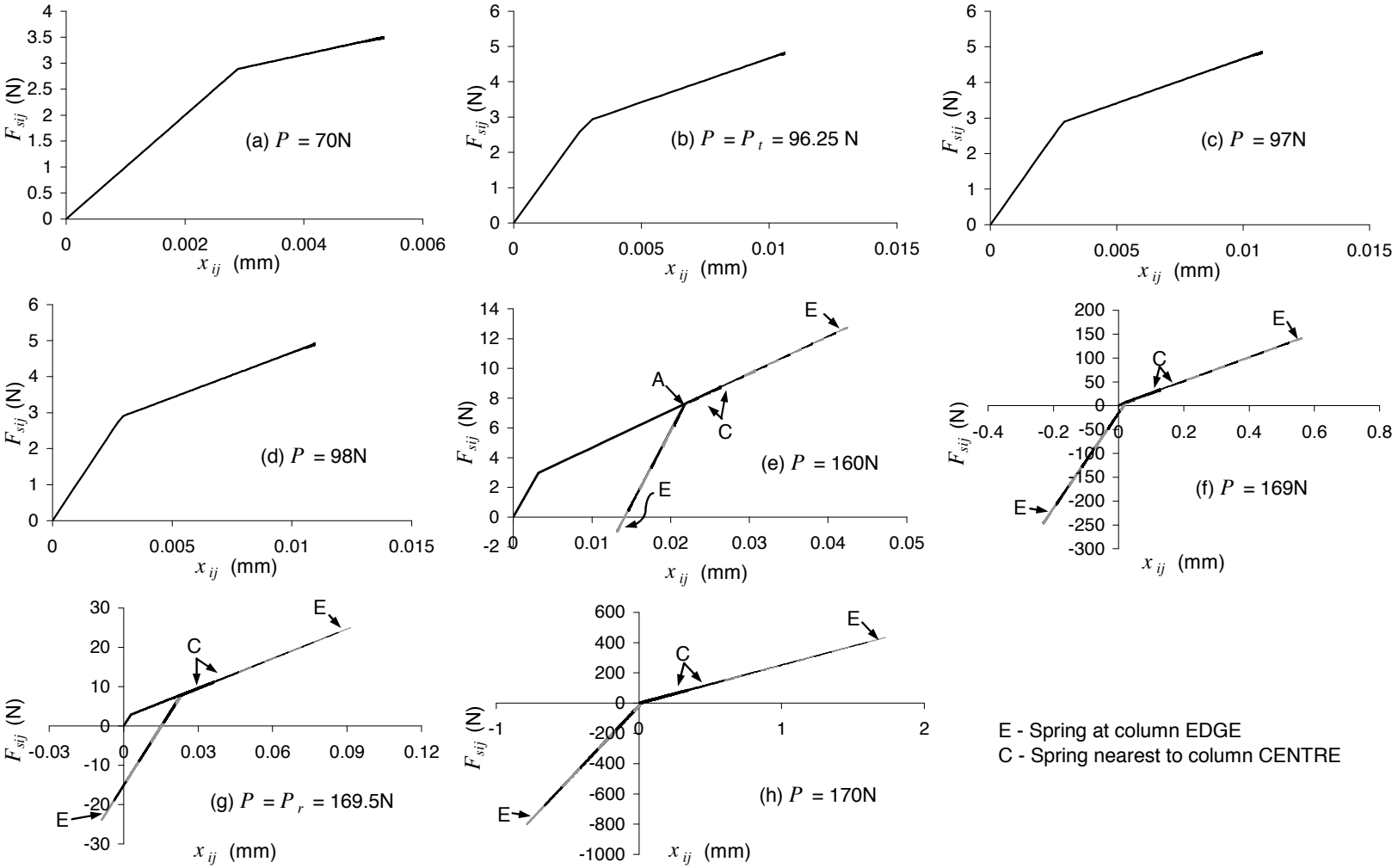

E - Spring at column EDGE
C - Spring nearest to column CENTRE

Figure16a

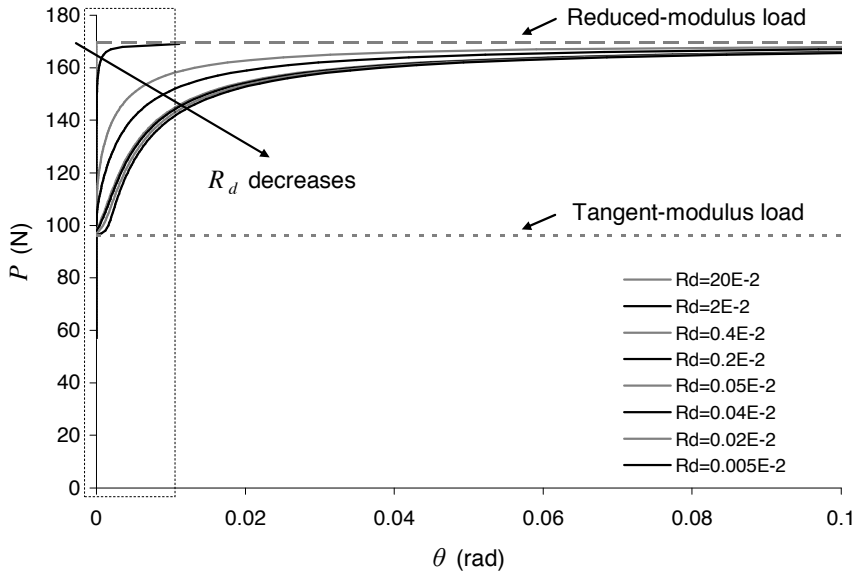
Reduced-modulus load
R_d decreases
Tangent-modulus load
P (N)
θ (rad)
Rd=20E-2
Rd=2E-2
Rd=0.4E-2
Rd=0.2E-2
Rd=0.05E-2
Rd=0.04E-2
Rd=0.02E-2
Rd=0.005E-2
0
20
40
60
80
100
120
140
160
180
0
0.02
0.04
0.06
0.08
0.1

Figure16b

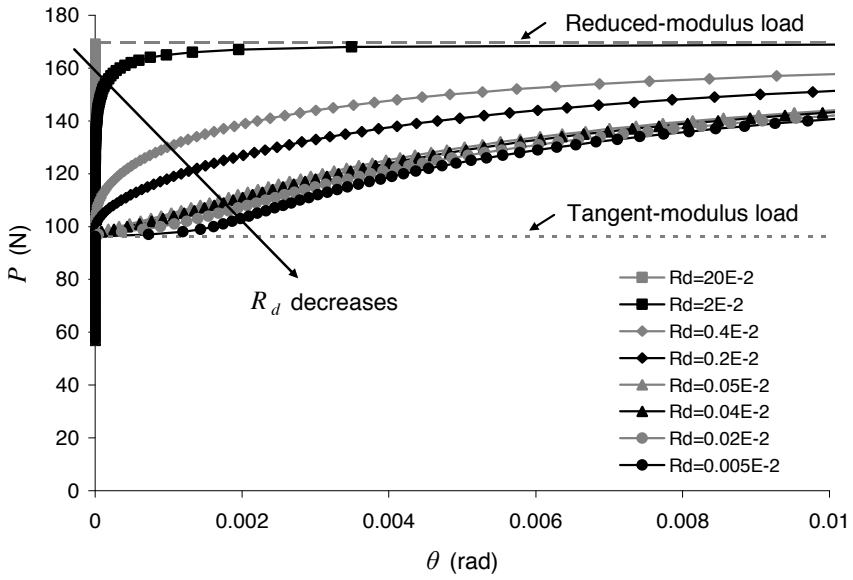
Reduced-modulus load
Tangent-modulus load
R_d decreases
P (N)
θ (rad)
180
160
140
120
100
80
60
40
20
0
0
0.002
0.004
0.006
0.008
0.01
Rd=20E-2
Rd=2E-2
Rd=0.4E-2
Rd=0.2E-2
Rd=0.05E-2
Rd=0.04E-2
Rd=0.02E-2
Rd=0.005E-2

Figure17

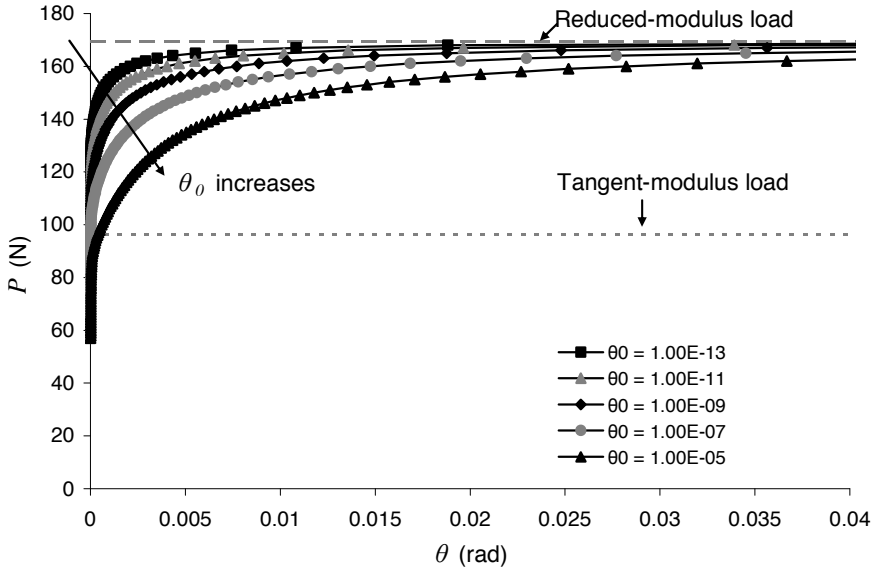
Reduced-modulus load
Tangent-modulus load
θ_0 increases
P (N)
θ (rad)
θ0 = 1.00E-13
θ0 = 1.00E-11
θ0 = 1.00E-09
θ0 = 1.00E-07
θ0 = 1.00E-05
0
20
40
60
80
100
120
140
160
180
0
0.005
0.01
0.015
0.02
0.025
0.03
0.035
0.04

Table1
Click here to download Table: huangtable01.doc

	α	β
Linear-elastic (L-E)	0	k
Plastic (P)	$F_p - k_t x_p$	k_t
Unloading (UL)	$F_{UL} - kx_{UL}$	k

Table2
Click here to download Table: huangtable02.doc

L (mm)	B (mm)	n	θ_0 (rad)	C_v (Ns/mm)	C_r (Nmms)	k (N/mm)	Δt (s)
500	10	10	1E-12	2000	2000	1000	0.005